

Are Sudden Stratospheric Warmings Generic? Insights from an Idealized GCM

MARTIN JUCKER

Program in Atmospheric and Oceanic Sciences, Princeton University, Princeton, New Jersey

(Manuscript received 19 November 2015, in final form 21 August 2016)

ABSTRACT

This work examines the life cycle of sudden stratospheric warmings (SSWs) from composites of a large number of events. The events are sampled from idealized general circulation model (GCM) integrations and form a database of several hundred major, displacement, splitting, and weak vortex events. It is shown that except for a few details, the generic zonal-mean evolution does not depend on the definition used to detect SSWs. In all cases, the composites show the stratosphere in a positive annular mode phase prior to the events and a barotropic response in the stratosphere at onset. There is a clear positive peak in upward Eliassen–Palm (EP) flux prior to the onset date in the stratosphere and a much weaker peak in the troposphere, making the evolution more consistent with the picture of the stratosphere acting as a variable filter of tropospheric EP flux, rather than SSWs being forced by a strong “burst” in the troposphere. When comparing composites of SSWs from the database with apparent influence at the surface (downward “propagating”) to those without such influence, the only significant differences are a somewhat more barotropic response at the onset date and longer persistence in the lower stratosphere after the onset for propagating SSWs. There is no significant difference in EP flux between propagating and nonpropagating events, and none of the definitions considered here shows a particular skill in selecting propagating events.

1. Introduction

Sudden stratospheric warmings (SSWs) are of major interest to the scientific community as they play a central role in stratosphere–troposphere coupling. For example, they seem to be linked to tropospheric blocking events (Woollings et al. 2010; Martius et al. 2009) and tropical dynamics (Kodera 2006; Gómez-Escolar et al. 2014), and they can induce long periods of negative tropospheric annular mode (AM) phase (Baldwin and Dunkerton 2001). Especially as a result of the latter, SSWs are hopeful candidates for seasonal forecasting (Sigmond et al. 2013; Tripathi et al. 2015).

Automatic detection based on one or more clearly defined criteria is important in many situations, such as comparing across many and/or large datasets, model

evaluation, forecasting studies, and large ensemble and/or long model integrations. However, reliable automatic SSW detection remains problematic, and even the exact definition is not unequivocal, as several classification criteria have been proposed in the literature (Butler et al. 2015).

Here, one can distinguish, among others, between major and minor events (Matsuno 1971; Schoeberl 1978; Labitzke 1981; Andrews et al. 1987), displacements and splitting events (Charlton and Polvani 2007; Mitchell et al. 2013; Matthewman and Esler 2011; Seviour et al. 2013), strong and weak polar vortex events (Baldwin and Dunkerton 2001; Polvani and Waugh 2004; Limpasuvan et al. 2004), or downward-propagating versus nonpropagating events (Nakagawa and Yamazaki 2006; Sigmond et al. 2013).

In this work we argue that in terms of zonal-mean evolution, there is little difference between the events selected by different definitions, similar to previous studies of reanalysis data (Coughlin and Gray 2009; Palmeiro et al. 2015). We also show that a strong tropospheric forcing prior to the event, although part of the life cycle, probably cannot be seen as the main trigger of SSWs.

Most of the work on sudden warmings is based on reanalysis products, or comprehensive historical general circulation model (GCM) simulations. As a result, on the

Current affiliation: University of Melbourne, Melbourne, Victoria, Australia.

Corresponding author address: Martin Jucker, School of Earth Sciences, and ARC Centre of Excellence for Climate System Science, McCoy Building, University of Melbourne, Melbourne VIC 3010, Australia.
E-mail: publications@martinjucker.com

DOI: 10.1175/JAS-D-15-0353.1

© 2016 American Meteorological Society. For information regarding reuse of this content and general copyright information, consult the [AMS Copyright Policy](http://www.ametsoc.org/PUBSReuseLicenses) (www.ametsoc.org/PUBSReuseLicenses).

order of 20–50 events are typically analyzed and further separated into smaller subcategories as described above. Because of the low number of events to analyze in observational datasets, it is difficult to quantify the differences between definitions and make robust statements about the general properties of a specific group of events.

One way to increase statistical confidence is to concentrate on a few events and run GCMs several times with slightly altered initial conditions, in order to create large ensembles of the same events with augmented statistical significance (e.g., Kuroda 2008; Gerber et al. 2009; Hitchcock and Simpson 2014). The caveat is that even though ensemble means can be statistically meaningful, they are still based on a few hand-selected events.

Another strategy is to perform long free-running model integrations, optionally in perpetual winter (e.g., Yoden et al. 1999). However, such studies are limited to the background climatology of the specific climate model used, which has been shown to influence the occurrence of SSWs (Taguchi 2016; Jucker et al. 2014).

The work presented here is complementary to reanalysis and comprehensive GCM studies, as it explores another route to producing statistically solid results: it takes advantage of the simplicity and low computational cost of idealized GCMs to produce a database of over 1500 events. In addition to very long integrations, the GCM is run with various stratospheric setups, such that there are not only a large number of events, but results also span over a wide variety of stratospheric equilibrium states. These different states of the stratosphere allow for a more general view of events, as they can be seen to mimic the different background states during the cold season (early, mid-, or late winter), the differences between the Northern and Southern Hemispheres, and the various biases in comprehensive GCMs. As a consequence, they allow us to determine what properties of SSWs are generic and not specific functions of one given climatology.

This is also of relevance in the ongoing effort of defining one generally accepted definition of SSWs, as it shows the consequences of selecting events according to one method or another. Any general definition will need to be applicable not only to reanalysis, but also model simulations, which might have slightly different climatologies, but are important tools to study basic mechanisms, as shown in the past (e.g., Polvani and Kushner 2002; Kushner and Polvani 2004; Charlton and Polvani 2007; Gerber and Polvani 2009; Hitchcock et al. 2013).

In the next section, the numerical model setup is discussed, and the autocorrelation time scales of the model are compared to reanalysis in section 3. Section 4 details the definitions of SSWs applied for this study, before discussing the composite evolution in section 5. Section 6 concentrates on the differences between

propagating and nonpropagating events, before concluding in section 7.

2. Numerical model and experiments

The idealized GCM used in this study, Jucker–Fueglistaler–Vallis stratosphere (JFV–strat), version 1.1.1, is described in detail in Jucker et al. (2014, hereafter JFV14), and we will only describe it briefly here. The code is freely available online (Jucker 2015a). It utilizes the spectral dry dynamical core of the Geophysical Fluid Dynamics Laboratory’s model hierarchy, version Riga, forced with the Newtonian cooling term

$$Q = -(T - T_e)/\tau, \quad (1)$$

where T is the temperature and T_e and τ are predefined relaxation temperature and time, respectively. Below 100 hPa, T_e and τ follow those of Held and Suarez (1994, hereafter HS94) with the addition of a north–south asymmetric term in the relaxation temperature to mimic solstice conditions (e.g., Polvani and Kushner 2002):

$$T_e^{\text{trop}}(\varphi) = T_e^{\text{sym}} + \varepsilon(\varphi) \sin\varphi, \quad (2)$$

where φ denotes latitude. Furthermore, the amplitude of the asymmetry ε takes on different values in the Northern (40 K) and Southern Hemispheres (10 K), as introduced in Jucker et al. (2013):

$$\varepsilon(\varphi) = \begin{cases} 40 \text{ K}, & \varphi \geq 0 \\ 10 \text{ K}, & \varphi < 0 \end{cases} \quad (3)$$

The model uses 40 levels up to 7×10^{-3} hPa, and we note that gravity wave drag is included with a crude Rayleigh damping above 50 Pa, exactly as in Polvani and Kushner (2002). A recent case study by Albers and Birner (2014) suggests that gravity waves can play an important role in SSW dynamics by modifying the polar vortex geometry prior to a given event. Such mechanisms cannot be included with our model.

The stratospheric T_e and τ are described analytically. Their exact form is given in JFV14 together with examples, and we give only a simplified form valid for the winter hemisphere. The most important difference with respect to many other Newtonian cooling setups in idealized models is that both the temperature and relaxation times are functions of latitude, height, and potentially time of the year (although this study only uses perpetual simulations). The main parameters of relevance here are as follows:

- The difference between winter solstice and equinox temperatures at 10 hPa and 90°N, henceforth denoted

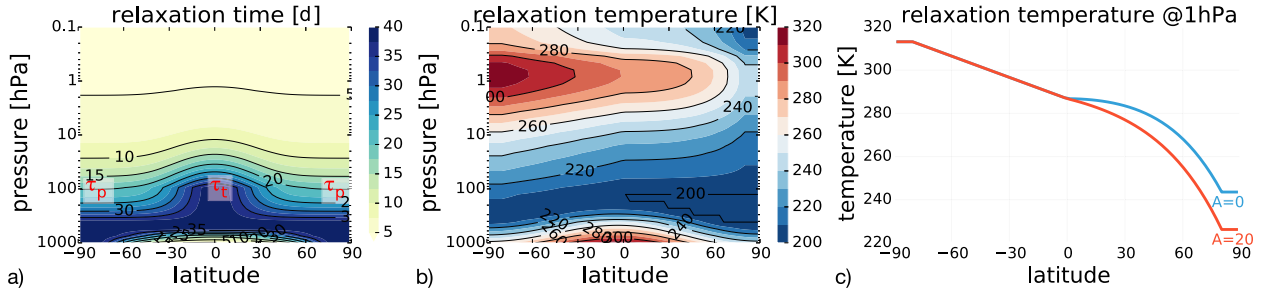


FIG. 1. Examples of (a) the relaxation time with $(\tau_t, \tau_p) = (40, 20)$ days, (b) the relaxation temperature with $A = 0$ K, and (c) the difference between $A = 0$ and $A = 20$ K at 1 hPa. In (a), we labeled the locations where τ_t (equator, 100 hPa) and τ_p (poles, 100 hPa) are defined. Note that there is a region of linear interpolation between the HS94 troposphere and JFV14 stratosphere between 350 and 100 hPa.

by A , and denoted by A_{NH}^1 in JFV14; A is given in kelvins, and the larger this number is, the colder the

polar night, and the larger the meridional temperature gradient in the winter hemisphere stratosphere:

$$T_{e,winter}^{strat}(\varphi > 0, p, d) = T_e^{EQ}(p)\Pi_T(\varphi, p) - \frac{A}{\delta p} \frac{\varphi}{90^\circ} \ln(p/100 \text{ hPa}) \cos(2\pi d/365), \quad (4)$$

where $T_e^{EQ}(p)$ is a predefined vertical profile at the equator and $\Pi_T(\varphi, p)$ is a fourth-order symmetric polynomial in latitude φ and logarithmic function of pressure p . In our simulations, $\delta p = -\ln(100 \text{ hPa})$ and $d = 0$ is the day of the year; see Fig. 1b for an example of T_e and Fig. 1c for the definition of A .

- The relaxation time scale in the tropical stratosphere, which is given as the value (days) at 100 hPa and denoted τ_t .
- The relaxation time scale in the polar stratosphere, which is again given as the value (days) at 100 hPa and denoted τ_p .
- These two parameters define the stratospheric relaxation time as

$$\tau^{strat}(\varphi, p) = \{\tau_p + (\tau_t - \tau_p) \exp[-(\varphi/30^\circ)^2] - 5d\} \times \Pi_\tau(p) + 5d, \quad (5)$$

where $\Pi_\tau(p)$ is a fourth-order polynomial of $\ln p$ with values of 1 at 100 hPa and 0 at 0.1 hPa. See Fig. 1a for an example of τ .

Figure 1 shows an example of a relaxation time setup of $(\tau_t, \tau_p) = (40, 20)$ days (Fig. 1a), a T_e setup with $A = 0$ K (Fig. 1b), and the definition of A via the difference of the meridional profile of T_e at 1 hPa for $A = 0$ and $A = 20$ K (Fig. 1c). In addition to these parameters, another difference to the setups of JFV14 is that we linearly interpolate between the HS94 troposphere and the JFV14

stratosphere, such that HS94 is used exclusively below 350 hPa and JFV14 is used exclusively above 100 hPa. This is done to avoid abrupt transition from the stratosphere to the troposphere at 100 hPa.

In addition to the stratospheric parameters A , τ_t , and τ_p , we will also vary the topographic forcing, which is again exactly as in JFV14, given by a cosine of longitude with a surface geopotential height Φ_0 of the form (Reichler et al. 2005; Gerber and Polvani 2009)

$$\Phi_0(\lambda, \varphi) = \begin{cases} gh \sin^2\left(\frac{\varphi - \varphi_0}{\varphi_1 - \varphi_0} \pi\right) \cos(m\lambda), & \varphi_0 < \varphi < \varphi_1 \\ 0, & \text{otherwise,} \end{cases} \quad (6)$$

where λ denotes longitude, g the acceleration of gravity, m the wavenumber of the topography, and h the “mountain height.” Parameters m and h are variable in this study, whereas $\varphi_0 = 25^\circ\text{N}$ and $\varphi_1 = 65^\circ\text{N}$ are kept constant.

The variable parameters for this work are then h and m for orographic forcing and A , τ_t , and τ_p for exploring a multitude of stratospheric setups. The detailed values for each of these parameters are as in JFV14 and are given in Table 1. We note here that the number of SSWs varies between the different setups. This is discussed in JFV14, with the most important result that there are generally more SSWs:

- the longer the relaxation time $\tau_{t,p}$,
- the higher the topography h , and

TABLE 1. Parameter settings for all setups: h denotes topography height, A the polar vortex amplitude in T_e at 10 hPa with respect to equinox configuration, and τ_l and τ_p low- and high-latitude relaxation times, respectively. All setups with $h > 0$ are run twice, once with wave-1 ($m = 1$) and once with wave-2 ($m = 2$) topography. (right two columns) The autocorrelation times at 100 hPa for both topographies (see Fig. 2).

h (km)	A (K)	τ_l (days)	τ_p (days)	act ₁ (days)	act ₂ (days)
0	0	40	20	72.3	72.3
1.5	0	40	20	24.9	20.5
3	0	40	20	26.1	41.4
5	0	40	20	17.1	20.5
3	20	40	20	34.5	40.5
3	15	40	20	23.7	39.2
3	10	40	20	21.2	35.7
3	5	40	20	24.6	42.3
3	0	30	20	24.5	33.7
3	0	20	20	44.5	44.0
3	0	10	20	42.4	39.0
3	0	30	10	33.0	33.1
3	0	30	30	25.6	32.7
3	0	30	40	26.4	34.3
3	0	20	30	22.8	40.9
3	0	20	40	23.4	40.0
3	0	40	30	22.4	30.8
3	0	40	40	20.3	35.3

- the warmer the polar night relaxation temperature (small A).

As expected, there are only very few SSWs when $h = 0$ (e.g., Kushner and Polvani 2005). We will, however, use all of the setups listed in Table 1 for the following discussions.

For each of the resulting 35 setups, a 2000-day spinup was followed by a 10 000-day integration period used for the analysis. We note that 2000 days is a very long spinup time, and a lot longer than actually needed for the model to achieve statistical steady state. Indeed, 500 days would have been sufficient, but since the number of integration days is not a limiting factor in this very lightweight model, we decided to run such long spinup periods.

3. Autocorrelation time scales

When studying atmospheric variability with a numerical model, it is important to check if the typical time scales related to internal variability are within an acceptable range compared to observations. Indeed, following the fluctuation–dissipation argument of Ring and Plumb (2007) and Gerber et al. (2008b), the autocorrelation time scale determines the response of the system to external perturbation, and a model can be unrealistically sensitive (or insensitive) to a given forcing (Chan and Plumb 2009).

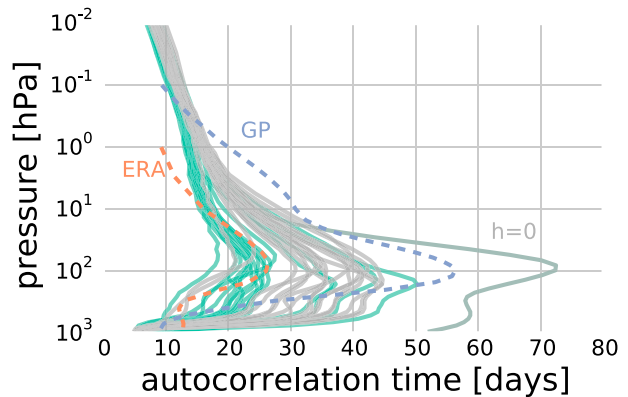


FIG. 2. NAM autocorrelation times for each vertical level (continuous), compared to ERA-Interim January NAM (red dashed) and GP (blue dashed). The model autocorrelation times are split into runs with wave-1 topography (green) and wave-2 topography (gray). In general, wave-1 topography has shorter time scales. The very long time scale is for the setup without any topographic forcing.

Gerber et al. (2008a) have shown that most of the comprehensive climate models used for the CMIP3 intercomparison have a long-time-scale bias, and a similar statement is true for the widely used idealized setup of Polvani and Kushner (2002), as discussed by Gerber and Polvani (2009, hereafter GP).

Although the tropospheric relaxation time remains unchanged in all simulations discussed here, stratosphere–troposphere coupling can have an effect on the characteristic time scale throughout the atmospheric column when changing the stratospheric setup. We apply the same analysis of the autocorrelation function of the first EOF of the geopotential (the annular mode) to compute the characteristic time scale as described in Gerber et al. (2008b). We plot the full vertical time-scale profiles in Fig. 2. For comparison, the profile for a simulation identical to integration 9 in GP (their “best” configuration), and ERA-Interim are also plotted. For reanalysis, the same approach as in Baldwin et al. (2003) and Gerber et al. (2008a) was used, and the average over the climatological January time scales was performed.

The autocorrelation time scales for the different simulations generally scale with their respective values at 100 hPa, which is given in the last two columns of Table 1. The one simulation with very long autocorrelation time scales of up to 72 days at 100 hPa is the setup without any topographic forcing. All other setups have fairly realistic autocorrelation time scales, spanning from smaller to larger than reanalysis. Note how the autocorrelation time scales are generally shorter with wavenumber-1 ($m = 1$, green lines) than with wavenumber-2 ($m = 2$, gray lines) orographic forcing,

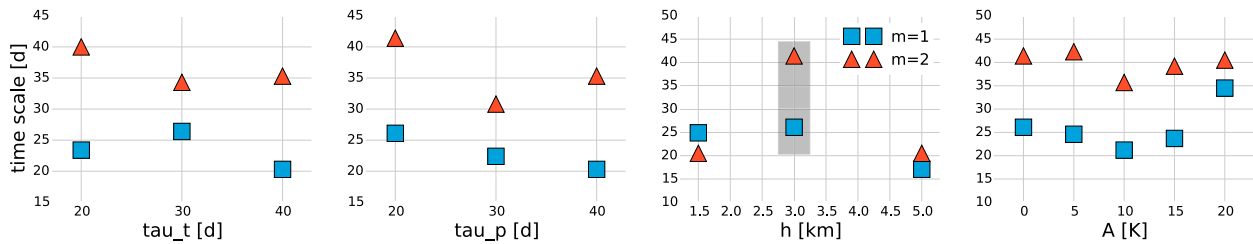


FIG. 3. Autocorrelation times at 100 hPa in the model runs as a function of τ_t , τ_p , h , and A . Blue squares ($m = 1$) and red triangles ($m = 2$) show a suite of runs where all parameters are kept constant except the one given on the x axis. The very long time scales of the $h = 0$ run have been omitted. (right center) The gray box illustrates the autocorrelation time spread of the complementary experiment, where all parameters except the one given on the x axis are varied. Note how this spread is just as large as the spread when changing any one parameter. In general, the only parameter that has control over the autocorrelation scale is the topography wavenumber m .

with the former generally closer to the autocorrelation time scales from reanalysis. While it is very encouraging that the autocorrelation time scales of this model can be very similar to reanalysis and represents a major improvement to the often used PK model, this work purposefully generates a wide range of setups to find more general results, while keeping the spread within reasonable values.

Figure 3 shows the autocorrelation times at 100 hPa, where they are longest and their spread is largest, as functions of the model parameters τ_t , τ_p , h , and A , in addition to $m = 1$ (blue squares) and $m = 2$ (red triangles). The panels show exclusively simulations where the only changing parameter is the one on the x axis, with the default parameters set to $\tau_t = 40$, $\tau_p = 20$, $h = 3$, and $A = 0$. The gray box in the third panel illustrates the spread of the complementary experiment—that is, when only one parameter is fixed and all others change. There are only very weak dependencies on any of the free parameters (other than m). Indeed, the large spread of the gray box shown in the third panel indicates that for any given value of one parameter, the annular mode time scale can vary just as much by changing the remaining parameters, as it would when changing that one parameter on the x axis (cf. vertical spread to spread of triangles and squares). In particular, there is no clear dependence of the annular mode time scales on the relaxation time scales, in agreement with earlier findings (Charlton-Perez and O’Neill 2010). Thus, other than the topography wavenumber m , no single parameter has control over the autocorrelation time scale, and at least for the range explored here, the relaxation times $\tau_{t,p}$ do not translate into the autocorrelation time.

4. SSW definitions

As there are different definitions of SSWs, this study will utilize three of the most widely used definitions. First, the so-called WMO criterion (Labitzke 1981),

which defines minor SSWs as events where the 10-hPa (or below) temperature gradient between 60°N and the North Pole becomes positive. It has become standard to only consider the pressure surface at 10 hPa, and not below, and the same is done here. Major events occur when in addition the zonal-mean zonal wind reverses at 60°N and 10 hPa.

Second, one can distinguish between displacements and splitting events, as in Charlton and Polvani (2007) and Mitchell et al. (2011). The exact criterion applied here follows closely Seviour et al. (2013), where displacement and splitting events are determined based on 2D moment analysis of the 10-hPa geopotential height field. Note that there is an ambiguity in the literature relative to the terms “splitting” and “displacement” events: Whereas Charlton and Polvani (2007) first look for wind reversal at 10 hPa and 60°N , and then distinguish between splitting and displacement events, the approach based on moment analysis does not impose any condition on the zonal wind. Therefore, it is possible that an event is classified as major sudden warming but satisfies neither the splitting nor displacement criteria defined above. On the other hand, it is also possible to classify an event as a displacement or splitting event but not as a major sudden warming. We will denote the displacement events by “M1” and splitting events by “M2” to recall that these definitions are based on 2D moment analysis. An M1 event occurs if the centroid latitude from moment analysis of the polar vortex is lower than 68°N for more than 7 days, and an M2 event is defined by an aspect ratio of 2.4 or larger for at least 7 days. Should both criteria apply, we attribute the event to the M2 category. Note that the threshold for centroid latitude is slightly higher than the 66°N proposed by Seviour et al. (2013). As these authors note, the choice is somewhat subjective, and the resulting composites are not sensitive to the exact value. But with a centroid latitude threshold that is slightly farther poleward, the M1

TABLE 2. Number of SSWs detected for each definition and the total number of distinct events.

Type	No. of SSWs	$m = 1$	$m = 2$
Major	872	457	415
Minor	1239	600	639
M1	549	393	156
M2	939	353	586
Weak vortex	1148	520	628
Total distinct (100 days)	1557	771	786

detection criterion becomes less restrictive and allows for similar event numbers as the other criteria.

Third, following Baldwin and Dunkerton (2001), a criterion can be defined based on the (standardized) annular mode index (i.e., of unit standard deviation, and subsequently referred to as “AMI”), with an SSW occurring when a predefined threshold is exceeded. To include not only the strongest events, this threshold is set to -2.0 standard deviations at 10 hPa as in Gerber and Polvani (2009) and not to an original (extreme) -3.0 standard deviations of Baldwin and Dunkerton (2001). We will refer to these events as “weak vortex” events in the following discussion.

For all definitions, the onset dates of two events have to be separated by at least 20 days to be counted as different events. Table 2 summarizes the number of SSWs detected for each definition and for all simulations listed in Table 1 and splits the total number into events detected for $m = 1$ or $m = 2$ orographic forcing. Major, minor, and all distinct (see definition below) events are almost equally distributed between $m = 1$ and $m = 2$, and weak vortex event numbers differ by about 20%. In contrast, 72% of all M1 events are generated with $m = 1$ topography, and 62% of all M2 events come from $m = 2$ simulations. Conversely, 28% of M1 events come from simulations with wave-2 ($m = 2$) and 38% of all M2 events from wave-1 ($m = 1$) topography. With $m = 1$ forcing, the M1/M2 ratio is about even, suggesting that this setup of the model might be somewhat closer to observations (Charlton and Polvani 2007; Mitchell et al. 2013). This is similar to section 3 (and in particular Fig. 2), where the $m = 1$ setup showed generally more realistic time scales.

The bottom row of Table 2 gives the number of distinct events: For a given event, any of the three definitions might yield a different onset date. Comparing the respective onset dates for all definitions, visual inspection showed that the same event can have a spread of onset dates of 30 days or more. Figure 4 shows one example of an event where the onset dates vary a lot, but we still consider this the same event as no sign of recovery is visible between the earliest (lag -33 days) and

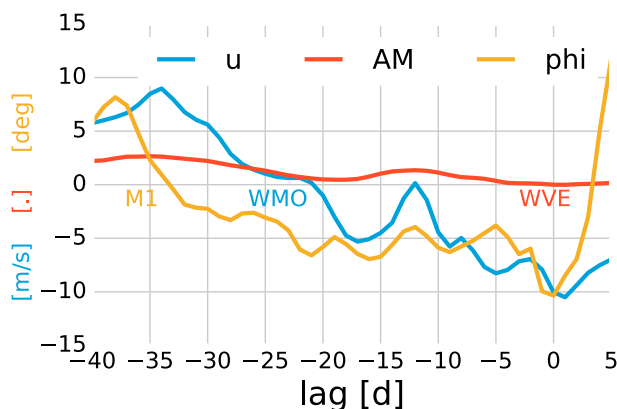


FIG. 4. Illustration of the possible spread between the onset dates of different SSW definitions. Plotted are the zonal-mean zonal wind at 60°N and 10 hPa (m s^{-1} , blue), the annular mode index $\text{AM}+2.0$ (red), and the equivalent polar vortex latitude ($\phi_e - 68^{\circ}$) ($^{\circ}$, yellow). The curves are adjusted such that the crossing of the zero line defines the respective onset date for each definition individually (M1 for displacement, WMO for major, WVE for weak vortex event). For this example, the different definitions yield onset dates of -33 (M1), -21 (WMO), and 0 (WVE). To compare across definitions, the global onset date is set to the day of minimum annual mode index, which is at $+1$ in this example. Note that the spread is usually on the order of a few days, and we chose an extreme example for illustration purposes here.

the latest (lag 0 days) definition of the onset date. It is important to note here that Fig. 4 represents a rare event, and in general the annular mode index minimizes within a short interval of the onset for M1/M2 and major/minor events. Even so, this behavior illustrates why it is important to have a large-enough sample to construct meaningful composites.

To get an estimate of the total number of independent events, we define a global onset date that is independent of detection criterion as the day of minimum annular mode index within the separation interval. This onset date will be used to construct all subsequent composites and comparisons. In addition, two distinct events have to be separated by at least 100 days. This is purposefully chosen to be rather long to make sure the analyzed events are indeed distinct. Even with this rather restrictive choice, 1557 SSWs were detected, giving an (ensemble) average of 1 SSW every 225 days, similar to the occurrence rate in reanalysis.

5. SSW evolution

In an attempt to study how much of the evolution of sudden warmings can be seen as “generic,” we create composites for major, displacement, splitting, and weak vortex events. In the composites we do not plot any data that is not statistically significantly different from zero at

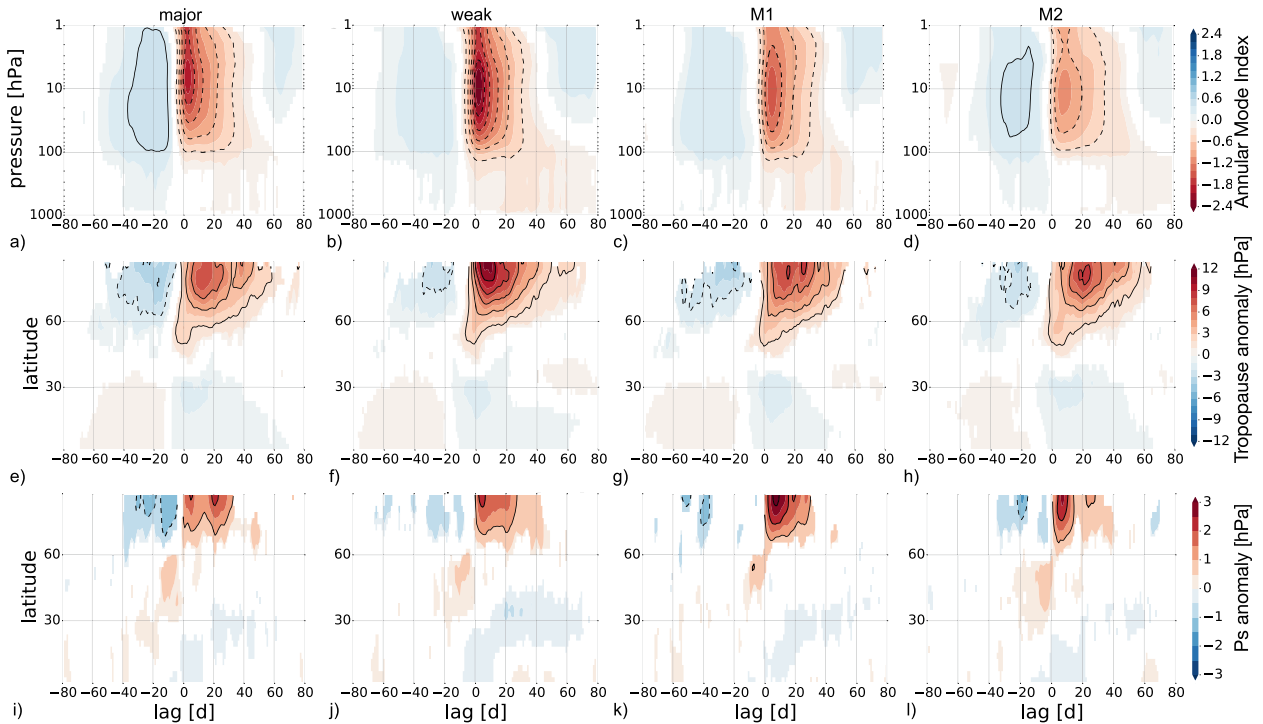


FIG. 5. Lag–pressure composites of (a)–(d) annular mode index, and lag–latitude composites of (e)–(h) zonal-mean anomalous tropopause height (hPa) and (i)–(l) anomalous surface pressure (hPa). (a),(e),(i) Major sudden warmings, (b),(f),(j) weak vortex events, (c),(g),(k) M1 events, and (d),(h),(l) M2 events. Although different in the details, the general evolution is similar for each definition. Black contour intervals are 0.4 for the annular mode index, 2 hPa for the tropopause, and 1 hPa for surface pressure. Negative contours are dashed.

the 5% level according to Student’s t test (i.e., white/not plotted in all subsequent figures).

a. Detailed evolution

Figure 5 shows the evolution of the annular mode index as a function of lag and pressure (top row) and the zonal-mean anomalies of tropopause height (hPa; middle row) and surface pressure (hPa; bottom row) as functions of lag and latitude. Here, the tropopause is defined as the lowest height where the lapse rate reaches values larger than -2 K km^{-1} . We define “anomalies” as deviations from background climatology of each simulation; that is, the fields from an event occurring during simulation n from Table 1 will be compared to the climatology of that same simulation n , and the composites are then built from all anomalous fields across all simulations.

In general, the evolution is very similar for all definitions, suggesting that all definitions capture similar events. This is in agreement with previous work applying various definitions to reanalysis (e.g., [Palmeiro et al. 2015](#)) or using an objective statistical k -means cluster technique ([Coughlin and Gray 2009](#)). As described earlier, the model’s autocorrelation times are generally

longer for $m = 2$ configurations, and those are also the setups with more splitting events (similarly with displacements and $m = 1$; see [Tables 1 and 2](#)). This could potentially lead to biases in comparing displacement composites with splitting composites in [Figs. 5c and 5d](#). However, performing the same composites for $m = 1$ and $m = 2$ separately yield results very similar to the composites shown here and do not show slower evolution for the $m = 2$ cases (not shown). We take this as an indication that even though the general autocorrelation times in the model vary as well as the frequency of SSWs, the evolution of the SSWs (once they happen) does not differ significantly.

We would like to remark on three further observations here. First, both the troposphere and stratosphere are in a positive AMI phase before the onset date. They are not in a neutral state, suggesting that there might be a phase before the onset date where the atmosphere is in a preferential state for an SSW to happen. (This point will be further examined in the discussion of [Fig. 9](#).)

Second, all annular mode composites show small signs of propagation into the troposphere, with the weak vortex and M1 events showing a slightly more negative annular mode in the troposphere between 20 and

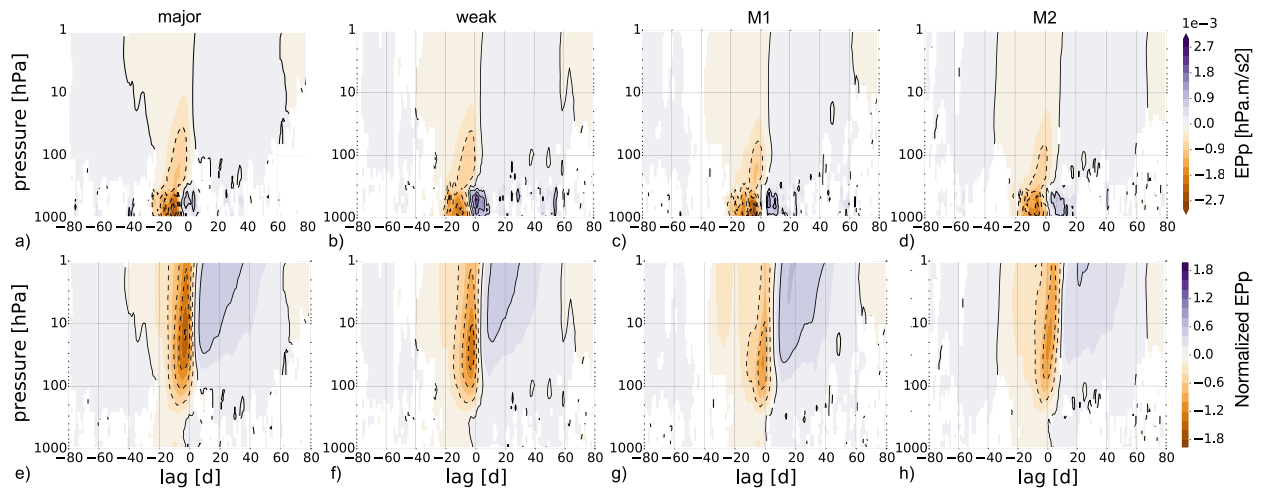


FIG. 6. Lag–pressure composites of (a)–(d) anomalous vertical Eliassen–Palm flux (hPa m s^{-2}) and (e)–(h) vertical Eliassen–Palm flux normalized to standard deviation. Both quantities are averaged between 20° and 90°N and negative values correspond to upward wave propagation (toward lower pressure). (a), (e) Major sudden warmings, (b), (f) weak vortex events, (c), (g) displacement events, and (d), (h) splitting events. Black contour intervals are 4 hPa m s^{-2} and 0.4 for the absolute and normalized vertical Eliassen–Palm flux. Negative contours are dashed.

60 days after the onset date. Thus, Figs. 5a–d indicate the presence of intensified stratosphere–troposphere and surface coupling after a “typical” SSW. The zonal-mean surface pressure anomalies (Figs. 5i–l) show a positive effect in all four composites after the onset date, confirming that some effect of SSWs can be expected on the surface. We will come back to the question of downward propagation in section 6.

A third observation is that in both surface and tropopause pressure, some indication of a seesaw between high and low latitudes is present, starting about 10 days before onset, and persisting at high latitudes for up to 60 days. The high-latitude tropopause is lower (higher pressure) in all composites during this period, and low-latitude tropopause is higher (lower pressure) during the first 20 days after onset. This can be understood as an effect of increased meridional overturning circulation, although it is interesting that the largest low-latitude tropopause anomalies are not seen in the tropics, but rather around 30°N —that is, over the subtropical jet. [Indeed, Fig. 9, which will be discussed in more detail later, confirms that a positive residual circulation anomaly builds up around 10 days before onset (brown shading).] This anomaly is strongest in midlatitudes and matches the above observations of anomalous tropopause height; anomalous upwelling (downwelling) in low (high) latitudes as depicted by stronger streamfunction coincides with anomalously low (high) tropopause (and surface) pressure.

Figure 6 shows the evolution of the anomalous vertical Eliassen–Palm flux component (EP_p ; Figs. 6a–d) and the same quantity but normalized to its standard

deviation (Figs. 6e–h). Both are weighted by the cosine of latitude and averaged for all latitudes north of 20° :

$$EP_p = \int_{20}^{90} f \left(\overline{\frac{v'\theta'}{\partial_p \theta}} - \left\langle \frac{v'\theta'}{\partial_p \theta} \right\rangle \right) \cos \varphi \, d\varphi \bigg/ \int_{20}^{90} \cos \varphi \, d\varphi, \quad (7)$$

where the angle brackets denote the time mean, f the planetary vorticity, φ latitude, v meridional wind, and θ potential temperature. Note that these plots are in pressure coordinates and EP_p is in units of hectopascal meters per squared second, such that negative values of EP_p correspond to upward wave propagation (i.e., toward lower pressure), similar to Edmon et al. (1980). With this definition, the (anomalous) zonal acceleration in the momentum equation due to the vertical component is simply the derivative $\partial_p(EP_p)$.

As before, the evolution for all definitions is very similar. At large negative lags, the upward EP flux is anomalously weak (purple shading) in the stratosphere but becomes anomalously strong (brown shading) around the time the annular mode phase reaches its maximum (note that again, even though the signal is weak, these features still are statistically significant). After this, around 40 days before the onset, there is a rapid strengthening of anomalous upward EP flux in the stratosphere. Starting around lags -20 to -10 days, a clear upward maximum occurs in the troposphere, similar to a “burst” in upward EP flux.

This burst should be put into perspective for two reasons. First, it occurs after upward EP flux in the upper stratosphere is already anomalously strong and should,

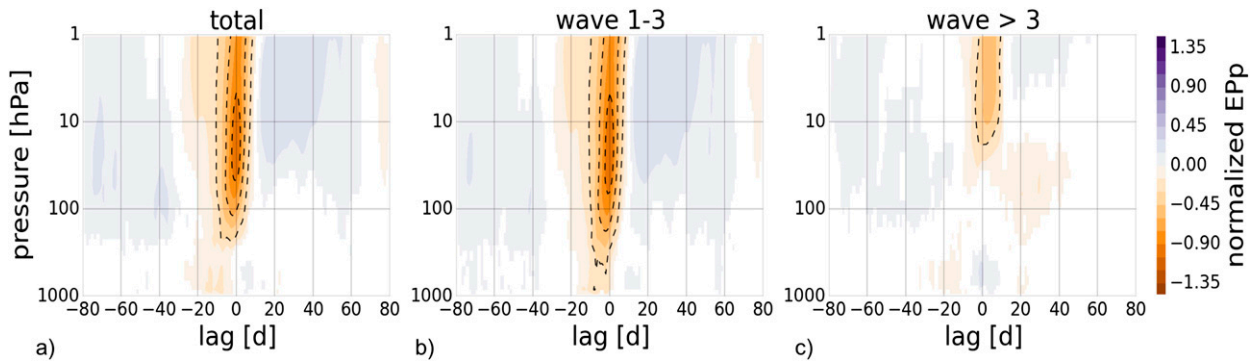


FIG. 7. Anomalous vertical EP flux from (a) all waves, (b) planetary waves (wavenumbers 1–3), and (c) smaller-scale waves (wavenumbers > 3). Anomalous vertical EP flux is normalized by the respective standard deviation in each panel and averaged from 20° to 90°N. This is as in Fig. 6, but now compositing all distinct SSWs. Note that the color scales and contours have been rescaled by a factor of 0.75 compared to Fig. 6. Clearly, increased anomalous vertical EP flux just before the onset date in the troposphere is dominated by planetary waves. The black contour interval is 0.3 and shading contour interval is 0.15.

therefore, not be seen as the cause of the SSW. Second, the troposphere has a large variability in the vertical component of EP flux, and it is not clear from these composites whether the observed increase in vertical EP flux is strong with respect to its local variability. We therefore normalize the composites by the standard deviation at each pressure level (Figs. 6e–h). These plots then suggest that while there is a relatively sudden maximum of upward EP flux, it is not particularly strong when compared to general tropospheric variability. We note that this general observation is true for both total EP flux and also when considering only planetary waves. Figure 7 shows the composite of all distinct SSWs (not separated by definition) for all waves (Fig. 7a), for planetary waves only (Fig. 7b), and for smaller-scale waves only (Fig. 7c). Wave activity in the stratosphere is generally dominated by the largest-scale waves, which is why the difference between planetary and all waves is very small in the stratosphere, with only a small contribution from higher wavenumbers at the beginning of vortex recovery, when very weak zonal winds allow smaller-scale waves to propagate higher into the stratosphere. In the troposphere, the main contribution clearly comes from planetary waves (Fig. 7b), starting about 10 days before the onset, which is then responsible for the EP flux peaks in the stratosphere at the onset date discussed above (Figs. 6e–h).

While the interplay between planetary waves originating in the troposphere and the changes in refractive index due to those waves breaking in the stratosphere certainly is intrinsically linked to the evolution of sudden warmings, Figs. 6e–h and 7 clearly show that the average increase in upward EP flux in the troposphere is much smaller than the local standard deviation. This means that tropospheric EP flux bursts cannot be the lone initiators

of SSWs, even if considering only planetary-scale waves (Fig. 7b). Indeed, one can expect many strong tropospheric EP flux events without subsequent SSWs.

We therefore argue that the stratosphere has to play an active role in the initiation of SSWs and is not simply reacting passively to tropospheric perturbations. In the proposed mechanism, the stratosphere has to provide an environment where perturbations from below are allowed to propagate upward and are directed in a way to be more “efficient” in decelerating the polar vortex when breaking in the stratosphere, and the troposphere can then be seen as a reservoir of planetary wave activity rather than the main decisive actor in the evolution.

To explore the behavior of other fields, Figs. 8 and 9 show the composite evolution of anomalous zonal mean zonal wind and the (anomalous) residual meridional circulation in addition to the anomalous EP fluxes described above. We also encourage the reader to consider the interactive version of Fig. 8 online (Jucker 2016a) for deeper understanding. Note that all these figures are based on composites of all distinct events and not separated into different definitions.

The anomalous zonal-mean zonal wind evolution is similar to the annular mode evolution described above, with stronger positive AM phase corresponding to a stronger and poleward-shifted polar vortex and vice versa. The seesaw in tropopause height and surface pressure seen in Figs. 5e–l is a consequence of the meridional circulation being anomalously weak at large negative lags (Fig. 9a) and anomalously strong between lag –20 days and the onset (Figs. 9b–d)—we note here that the composite of Fig. 9d is dominated by the strong response around the onset, confirming our earlier assumption.

The strengthening of the polar vortex at negative lags coincides with a sharpening of the potential vorticity

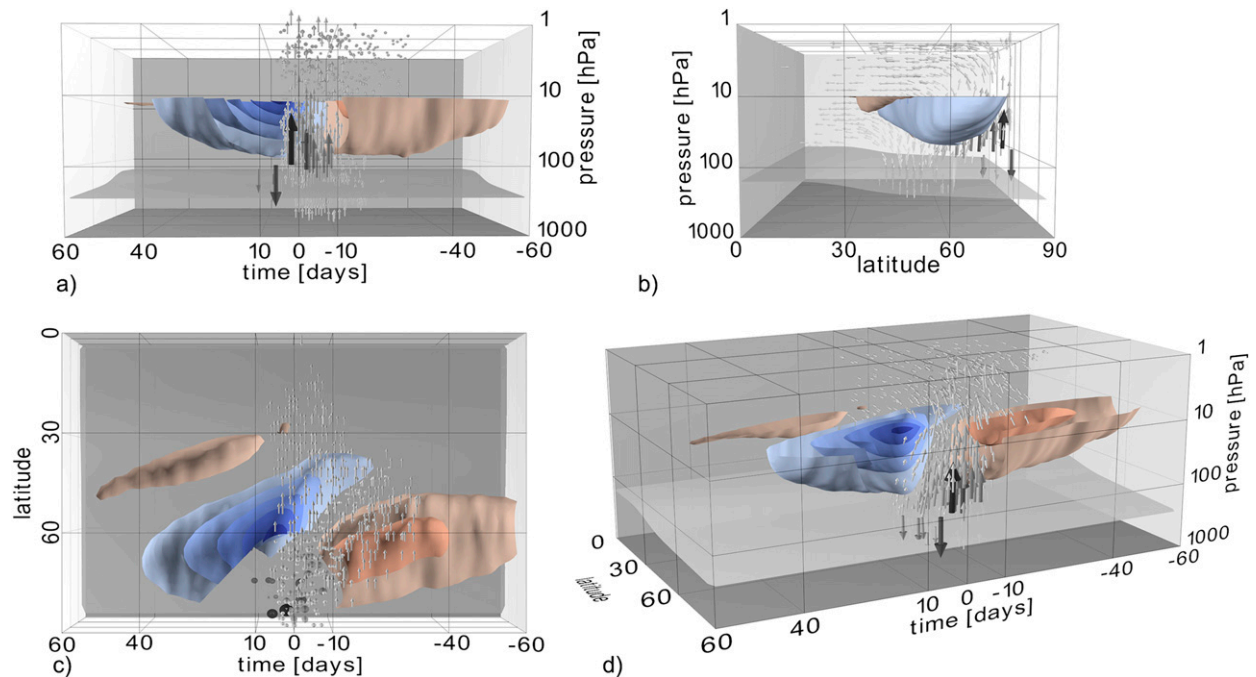


FIG. 8. Three-dimensional Hovmöller-like diagram of the composite zonal-mean evolution of major sudden warmings. The views are from (a) the side, with time from right to left and latitude into the picture plane (North Pole in the close plane, equator in the back); (b) the front, with latitude from left to right, time decreasing into the picture plane; (c) the top, with time running from right to left, latitude from top to bottom, and pressure into the picture plane; and (d) a free position, with time running from right back to left front, and latitude from left back to right front. The pressure is from bottom to top in all panels except (c), where it is in the picture plane. The red and blue isosurfaces are cut around the onset date for clarity and show anomalous zonal-mean zonal wind, with surface intervals of 2 m s^{-1} . Clearly visible is a strengthening and northward propagation (sharpening) of the polar vortex prior to the onset and a strong weakening during and after the onset. The weakening starts in midlatitudes around 20 days before the onset (northward shift of the polar vortex) and peaks around 60°N at the onset date. The arrows show anomalous Eliassen–Palm flux, scaled to the average EP flux, and are only shown where it is more than 10% higher than average. Color and size are proportional to the magnitude of the anomalous EP flux vectors. It has a positive component at the surface midlatitudes around 10 days prior to onset (and 30 days after the polar vortex starts to strengthen) and is maximum around the onset date in the lower stratosphere. The gray transparent surface shows the tropopause. An interactive html version can be downloaded at [10.5281/zenodo.46174](https://doi.org/10.5281/zenodo.46174) (Jucker 2016a). Created with pv_atmos (Jucker 2014).

(PV) gradient \bar{q}_ϕ at the vortex edge. Figure 10 shows anomalous \bar{q}_ϕ averaged between lags -40 to -20 days (top) and lags -20 to 0 days (bottom), together with anomalous EP flux vectors, for each SSW detection method separately. One can clearly see that there is a sharpening of the PV gradient around 60°N before the appearance of anomalously large EP flux and, in particular, long before the strong upward flux in the troposphere. This evolution is compatible with the idea of a “tuning” of the stratosphere in a resonant state (Albers and Birner 2014; Matthewman and Esler 2011; Esler and Matthewman 2011; Dritschel and McIntyre 2008; McIntyre 1982): The sharpening of the PV gradient increases the refractive index locally and, therefore, redirects the EP fluxes and focuses them toward higher refractive index, which means onto the edge of the polar vortex. It matches the observations of Matthewman and Esler (2011) particularly well, as those authors also observed that the tropospheric influence in triggering an

SSW is much less important than generally thought. It also supports the idea that while wave forcing from the troposphere has to be present, the state of the stratosphere is the determining factor for the occurrence of SSWs, and the troposphere merely serves as a reservoir of the necessary perturbations.

Figure 10 shows that even in terms of local (in latitude–pressure and time) PV gradient evolution, the events detected by the different methods behave very similarly; that is, the PV gradient sharpening appears to be a general characteristic of SSW evolution. This is somewhat different to Albers and Birner (2014), who focused on splitting events when discussing PV gradient sharpening.

b. Discussion

We now put together all the detailed observations from Figs. 5 to 10 into a unified description of the zonal-mean evolution.

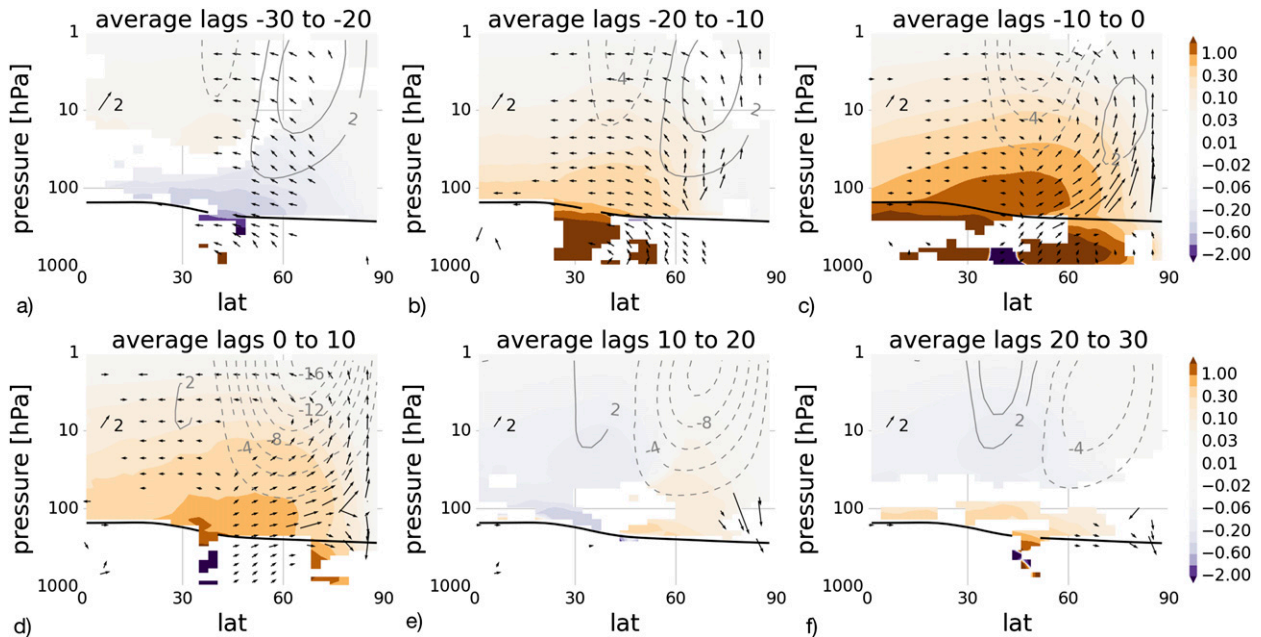


FIG. 9. Two-dimensional temporal slices of Fig. 8, with additional averaging performed over 10-day periods. In addition to the anomalous zonal wind and EP flux depicted in Fig. 8, anomalous residual-mean streamfunction has been added (shaded contours). Anomalous zonal wind contour interval is 2 m s^{-1} , with solid (dashed) indicating positive (negative) values, and every second contour is labeled. Note that here zonal wind anomalies are plotted up to 1 hPa, whereas they are only included up to 10 hPa in Fig. 8. For the streamfunction ($1 \times 10^9 \text{ kg s}^{-1}$), positive values (brown) imply clockwise circulation. Note the logarithmic color scale for the streamfunction as indicated by the color bars. The EP flux arrows are proportional to the anomalous EP flux normalized to climatological EP flux, and the arrow near 10 hPa and 5°N labeled “2” shows a reference length of 2.

There is a strengthening of the polar vortex and a weakening of upward EP flux in the stratosphere, accompanied by a slight decrease in stratospheric Brewer–Dobson circulation, at lags anywhere between 20 and 60 or more days before the onset date (Figs. 6, 8, and 9). The anomalous upward EP fluxes switch sign around the same time that the positive AM phase reaches its maximum (Figs. 5a–d and 6). This happens first and most strongly in the stratosphere above 10 hPa, at lag -30 to -40 days, and around the same time the meridional PV gradient starts to sharpen around the polar vortex edge.

Once the upward EP flux increases and the polar vortex starts to weaken, a process that might be thought of as a positive feedback appears, with the polar vortex weakening and the EP flux strengthening more and more until the onset date, when the feedback is broken as the zonal wind changes sign, and both the AM and vertical EP flux anomaly change sign once again, but much faster this time.

The anomalous tropopause height follows the sign of the anomalous residual circulation, with a seesaw between low and high latitudes, and the surface pressure evolution is consistent with the idea that the tropospheric circulation and surface impact follow from tropopause height variations and eddy feedbacks (Lorenz

and DeWeaver 2007; Simpson et al. 2009; Hitchcock and Simpson 2014; Kidston et al. 2015).

6. Downward propagation

As mentioned in the introduction, a large part of the interest in SSWs comes from their apparent power to influence the state of the troposphere for several weeks or even months, and we will concentrate on this phenomenon in this section. We will call SSWs that show a change in tropospheric circulation toward negative annular mode phases after the onset date “propagating” SSWs, and all other events will be “nonpropagating.” We will try to find distinct differences between propagating and nonpropagating SSWs and identify recognizable characteristics that allow for a categorization, and possibly prediction, of each event. However, we will show here that even though some differences between propagating and nonpropagating SSWs can be found, most depend on the exact definition of propagation, and they do not allow prediction.

There is no clear definition in the literature of when exactly an SSW is downward propagating. As with the definition of SSWs themselves, some decision has to be made as to when to call an event a downward-propagating

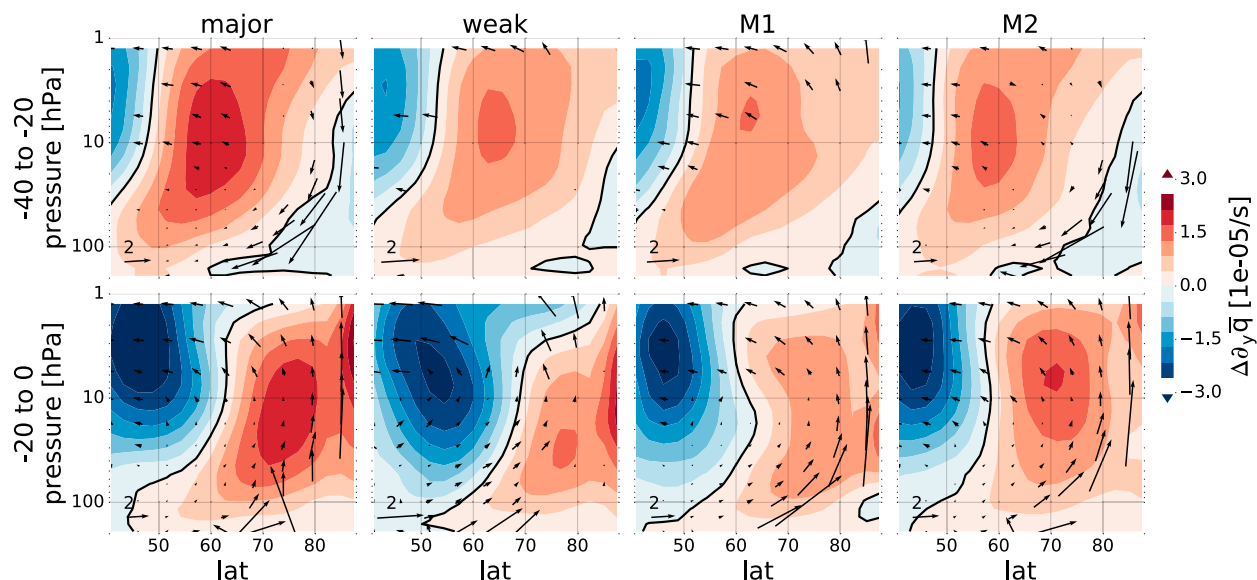


FIG. 10. Composites of meridional potential vorticity gradient anomaly ($1 \times 10^{-5} \text{ s}^{-1}$, actual minus climatological) for (left)–(right) major SSWs, weak vortex events, M1 events, and M2 events (shading, continuous line separates negative and positive anomalies). Arrows denote the normalized anomalous EP fluxes where statistically significant at the 95% level. A reference vector of length 2 is added near 45° and 110 hPa. (top) A clear steepening of the PV gradient happens already at lags -40 to -20 days, whereas (bottom) the anomalous EP fluxes from the troposphere only become large after lag -20 days.

event. Naturally, the idea of propagation of some kind of signal from the stratosphere into the troposphere comes from the “dripping paint” plots in Baldwin and Dunkerton (2001) (and Fig. 5 of this article), showing a negative phase of annular mode index that appears to propagate from the stratosphere into the troposphere. So the definition for propagation here will be based on the AMI in the troposphere and a certain proximity to an SSW in time.

a. Absolute threshold

In addition to inducing a negative phase of the annular mode, we are interested in events that do so for a considerable amount of time. Thus, for a first definition we perform a time average in the troposphere for separating purely coincidental days of extreme AMI from more persistent periods. Furthermore, to allow the downward propagation to proceed into the troposphere, a minimum lag should be observed before checking for extreme AMI values.

Based on these considerations, the first analysis applies the following definition for a propagating SSW:

Definition 1: If the average AMI at 500 hPa between 10 and 40 days after the onset day of an SSW passes below -0.6 , that particular SSW is considered propagating.

We remind the reader that the AMI is normalized to its standard deviation. The onset day is defined as the first day the AMI at 10 hPa passes below -2.0 , and all SSWs

not satisfying definition 1 are considered nonpropagating. This particular threshold value represents a compromise between having a considerable number of propagating SSWs (25% of the 1557 distinct events), while still having an appreciable effect in the troposphere (just over half a standard deviation over 1 month).

It is worth noting that we have also tried a propagation definition based on the running-mean annular mode index instead of a time average over a fixed lag period, but again the qualitative analysis remains the same.

Figure 11 shows the resulting composites. We are now interested in the differences between propagating and nonpropagating events, and we therefore test the statistical significance of the difference between the two, not the significance of each population compared to climatology, as done in the previous section. Therefore, data are only plotted where the propagating composite is significantly different from the nonpropagating composite at the 95% level according to Student’s t test.

By construction, the annular mode is in a strong negative phase between lags 10 and 40 days in the propagating case (left column). There is a small (but significant) negative phase in the troposphere already before the onset date, which suggests a tendency of the troposphere to already be at least close to a negative phase before the onset of the SSW, and the latter simply amplifying this tendency. In both cases, the stratosphere is in a positive AM phase before the onset in the composite, similar to the general results of the previous

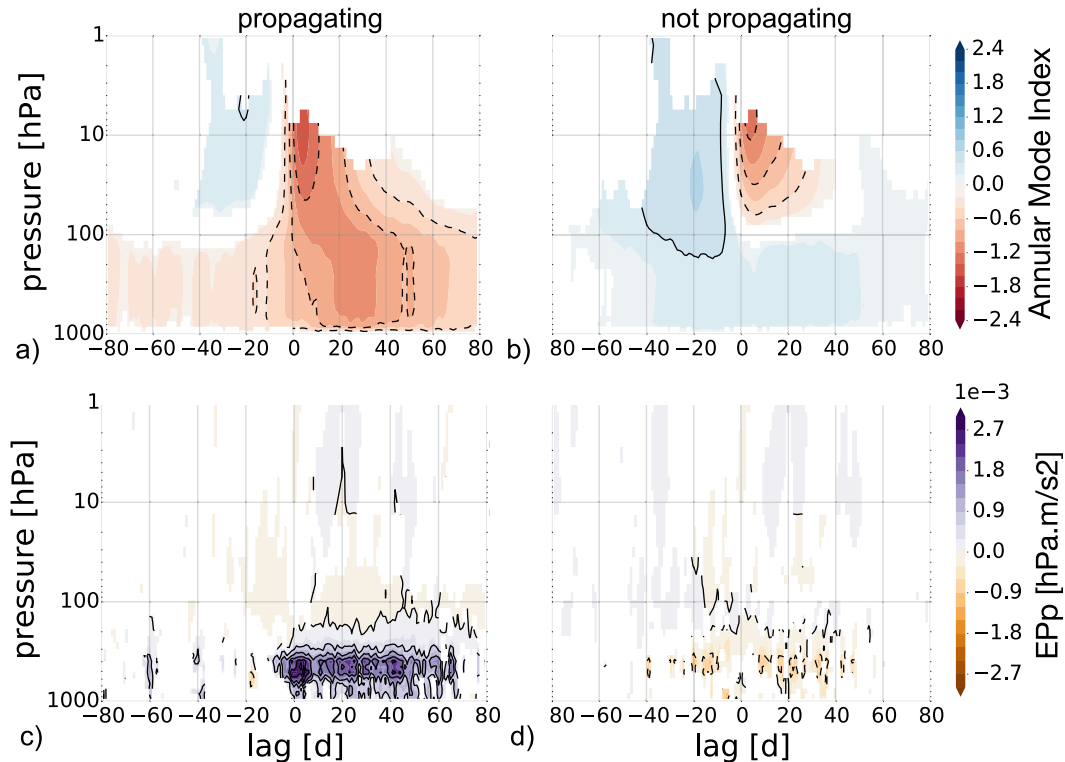


FIG. 11. (a),(b) Annular mode index and (c),(d) vertical component of the EP flux (hPa m s^{-2}) evolution for (a),(c) propagating and (b),(d) nonpropagating SSWs, as defined using a threshold of average annular mode index at positive lags (see text for details). Data are only plotted where the difference between the two is statistically significant at the 95% level and also significantly different from zero. By construction, AMI is in a negative state between lags 10 and 40 days in the propagating case. There is virtually no difference in upward EP fluxes at negative lags.

section, but the nonpropagating SSWs (right column) are in a significantly stronger positive phase in the lower stratosphere than the propagating composite. The fact that the nonpropagating composite shows a slightly positive AM phase in the troposphere at positive lags simply reflects the fact that most of the events with negative AM phase are included in the propagating composite, and the ensemble mean therefore has a tendency to be positive.

There is no difference in the evolution of the upward Eliassen–Palm (EP) flux (Fig. 11, bottom) between the two composites at negative lags. In particular, there is no significantly stronger tropospheric burst in the propagating case, which is in agreement with the earlier discussion of the role of tropospheric perturbations in SSW triggering. At positive lags, the anomalous downward EP flux (or positive EP_p) in the troposphere for the propagating cases is similar to observations from earlier studies by Garfinkel et al. (2013) and Simpson et al. (2009), according to which eddy–zonal mean flow feedbacks that are internal to the troposphere are essential to define the tropospheric response to stratospheric variability.

The clearest differences between propagating and nonpropagating events are an extended persistence of negative AMI in the lower stratosphere, a stronger positive AM phase in the lower stratosphere prior to the onset for nonpropagating events, and a more barotropic evolution at the onset for propagating SSWs (the latter can be inferred from the fact that the propagating AMI response at the onset is significantly stronger in the lower stratosphere than the nonpropagating AMI response). This is in agreement with earlier studies by Hitchcock et al. (2013), Hitchcock and Simpson (2014), and Seviour et al. (2016). Both the more barotropic nature and the persistence in the lower stratosphere of propagating SSWs result in a stronger annular mode anomaly in the lower stratosphere and, in particular, close to the tropopause. Thus, these events have a stronger effect in the tropopause region, which allows for better coupling to the surface (Lorenz and DeWeaver 2007; Hitchcock and Simpson 2014).

A secondary observation is that the troposphere seems to be in a preferentially negative annular mode phase already prior to the onset date, suggesting that at

least some of the captured events with this definition are in a negative AM phase in the troposphere independently of the occurrence of an SSW.

From these observations, one might conclude that the most prominent difference between propagating and nonpropagating events is the AMI signal at the onset and positive lags close to the tropopause, with propagating events showing a stronger and more persistent negative AMI than nonpropagating events. However, there is little to no predictive power at negative lags.

b. Relative threshold

A second approach to defining propagation is to consider the relative change in annular mode index in the troposphere after a sudden warming, as opposed to an absolute threshold of the annular mode. Figure 12 shows the distributions of the daily annular mode index at 500 hPa 1–80 days prior (blue) and 1–80 days after the onset date (red). Also shown are the mean μ , standard deviation σ , and skewness γ of the respective distributions. There is an average shift of the (mean) annular mode index after the sudden warmings of about -0.1 , switching sign from a slightly positive (negative lags) to a negative mean value (positive lags). It is interesting that the standard deviation of the AMI also decreases (from 1.0 to 0.97). This can be explained in part by the fact that there are fewer positive extreme events at positive lags, but it is also evident that although the troposphere is in a more negative state after sudden warmings in the mean, the most extreme negative AMI events do not become more frequent (there is little to no difference in PDF below -2.0).

Based on this observation, we define a second criterion for propagation:

Definition 2: The mean annular mode index at 500 hPa decreases by at least -0.1 from before to after the event; that is,

$$\langle \text{AMI}(t > 0) \rangle - \langle \text{AMI}(t < 0) \rangle \leq \Delta \text{AMI}, \quad (8)$$

where t denotes lag with respect to the onset date, angle brackets denote the time mean over all positive or negative lags (here up to 80 days), and ΔAMI is the threshold to define propagating events. As stated above, we use $\Delta \text{AMI} = -0.1$ as the threshold here. We tried various threshold values from -0.1 to -1.0 and other than smaller numbers of propagating events, the qualitative results remain the same. This criterion defines 759 events as propagating (49%). We can have a somewhat more permissive threshold with this definition than the previous definition, as we know that there was a shift in AMI around the onset date, whereas before we had to choose a rather restrictive threshold to be sure to capture more extreme events.

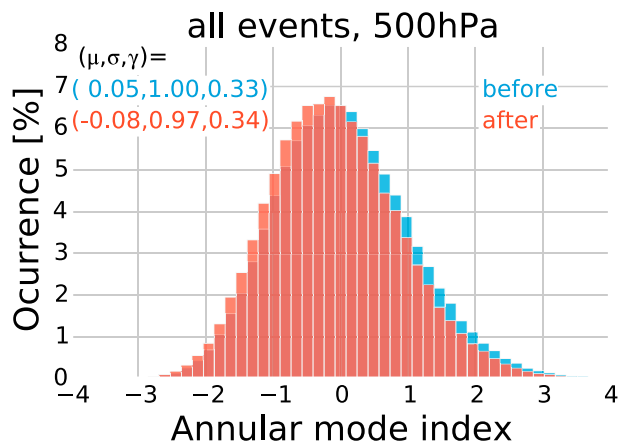


FIG. 12. AMI distribution at 500 hPa for all 1557 distinct events, divided into positive (red) and negative (blue) lags. Also shown are the values for the mean μ , standard variation σ , and skewness γ for the two populations. The mean of the population corresponding to positive lags is more than 0.1 lower (and negative) than the (positive) mean of the negative lags. The standard deviation of the days after the event is slightly smaller than before the event, such that although the mean has shifted from positive to negative, the most extreme negative events are not more frequent.

Figure 13 is equivalent to Fig. 11 but uses the second definition for propagating events. The composites confirm that as found above, at the onset date, the stratospheric annular mode signal for propagating events is stronger below 10 hPa and somewhat deeper than for nonpropagating events. However, there are also important differences from what we found before. In the propagating composite, there is now statistically significant increase in upward EP flux before the onset (Fig. 13c). It is interesting that there is a clear correspondence between the signs of anomalous upward EP flux and annular mode index; positive annular mode shows increased upward EP flux, whereas negative annular mode coincides with decreased upward EP flux. This is similar to findings of Polvani and Waugh (2004), but a cause-and-effect relationship cannot be inferred here. We also note that if we divide the anomalous upward EP flux by its standard deviation as in Fig. 6, this tropospheric signal all but vanishes.

Even though the propagation definition in (8) has no condition on a change of sign of the annular mode index, Fig. 13 indicates that most events do change sign and evolve from a positive AMI phase to a negative AMI phase. It is interesting to note that whereas previously (Fig. 11) we found that nonpropagating events show a somewhat stronger positive phase of the stratosphere prior to the onset, we now find that the stratosphere is in a stronger positive AMI phase prior to the onset in the propagating composite as compared

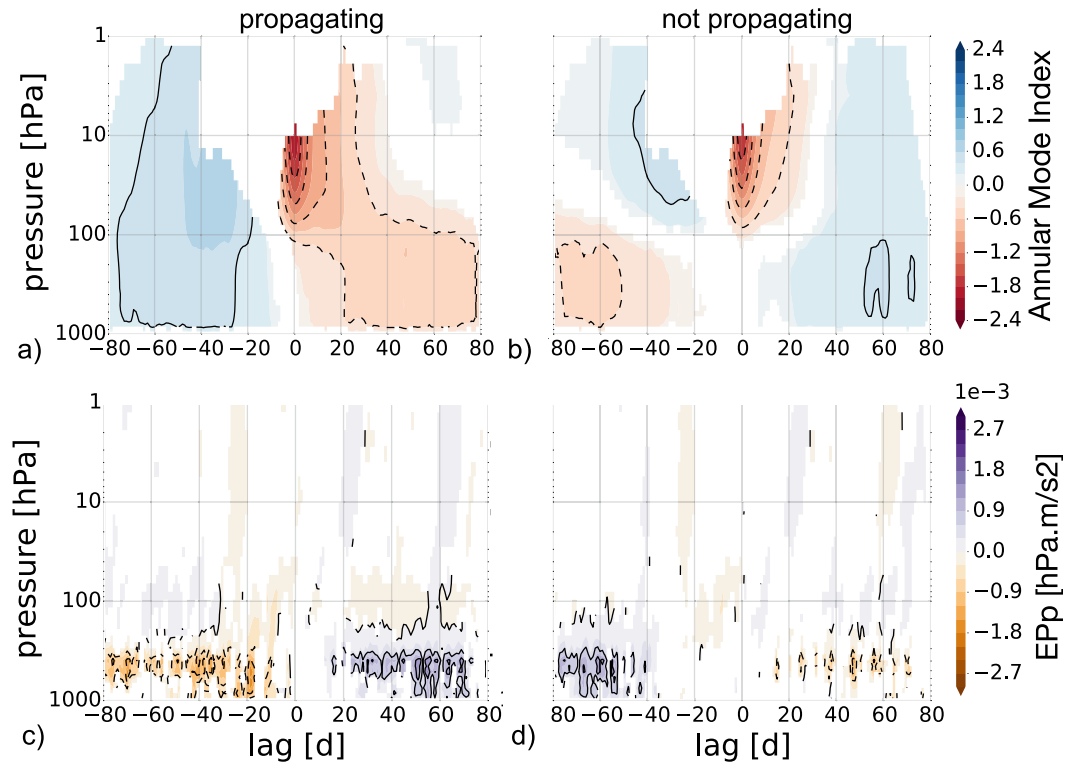


FIG. 13. (a),(b) Annular mode index and (c),(d) upward EP flux evolution for (a),(c) propagating and (b),(d) nonpropagating SSWs, as defined by a negative shift of the annular mode index in (8). Data are only plotted where the difference between the two is statistically significant at the 5% level and also statistically significantly different from zero. See text for discussion.

to the nonpropagating composite. This casts doubt on the robustness of the results before the onset date and therefore the prospects of predictability, as we discuss now.

c. Discussion

The two rather different results, particularly the evolution prior to the onset, from applying two different definitions of propagation into the troposphere show that it is difficult to find general characteristics of the phenomenon of “propagation” of sudden stratospheric warmings. On one hand, it is not obvious how to precisely define what we mean with propagating events. On the other hand, our study shows that the resulting composite evolution depends on the chosen definition, in particular at negative lags. There are, however, three more solid results:

- We could not extract any predictive skill at negative lags. Even though there are statistically significant signals in our general SSW composites at negative lags (see previous section), there is no significant difference between propagating and nonpropagating events before the onset date. The rather large differences of

the composites in Figs. 11 and 13 at negative lags is consistent with earlier findings that models have some skill in predicting propagation if initialized at the onset, but there is no predictive skill prior to the event (e.g., Sigmond et al. 2013).

- Once an event occurs, propagating SSWs consistently show a stronger signal in lower-stratospheric AMI at the onset. The negative AMI in the region just above the tropopause then also persists for a longer time. Thus, the instantaneous behavior at the tropopause at the onset can be seen as the most significant difference between propagating and nonpropagating events, and the evolution higher up in the stratosphere seems much less important.
- We observe a strong correspondence between the AMI and anomalous upward EP flux: there is more upward EP flux when the AMI is positive, and less if the AMI is negative. This observation, paired with the above point, indicates that internal tropospheric eddy feedbacks are more important than external stratospheric forcing in setting the persistence of the annular mode once an initial perturbation from the stratosphere is received at the onset. This is consistent with previous work concerning the determination of the

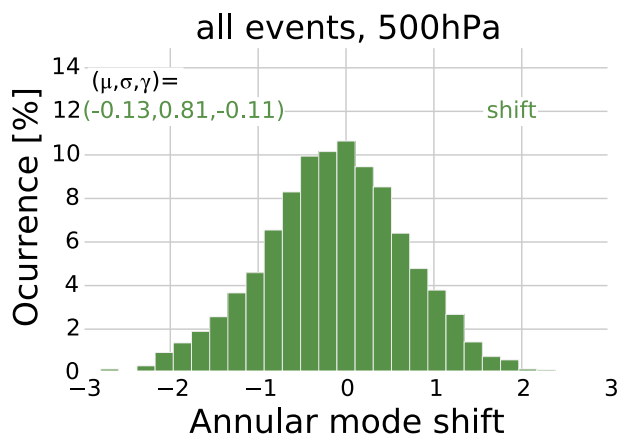


FIG. 14. Distribution of mean shift of AMI between positive and negative lags. There is no indication of a bimodal structure, giving support to the idea that there is no structural difference between propagating and nonpropagating events.

tropospheric jet latitude by [Simpson et al. \(2009\)](#) and [Garfinkel et al. \(2013\)](#).

As another way of looking at the problem, it is worth considering the annular mode PDF, as discussed in [Fig. 12](#), once more. [Figure 14](#) plots the PDF of the difference between mean AMI at positive and negative lags including all SSWs, with negative values meaning a shift toward lower AMI after the event. In agreement with [Fig. 12](#), the distribution has a mean around -0.1 and, most importantly, it shows a very Gaussian form; there is no hint of a bimodal structure. If there was a distinctive and clearly separate type of SSW that propagates, and one that does not, one would expect a bimodal distribution, with one peak corresponding to propagating events and the second peak representing nonpropagating events. But [Fig. 14](#) does not allow identifying two separate peaks in the PDF. Thus, either a distinct type of SSW that propagates exists but has a very small average effect on the troposphere (and can therefore hardly be called propagating), or there simply is no distinct type of SSWs that propagates. The Gaussian nature of the distribution rather suggests that there is only one type of SSWs which sometimes happens to propagate. It also explains why our results are not sensitive to the exact choice of the thresholds, as it captures a smaller or larger portion of the tails, rather than a distinctive secondary peak of the distribution.

To test whether one of the SSW definitions applied here is preferentially detecting propagating events, we split the propagating events according to their respective detection criterion and compute the conditional probability of propagation in [Table 3](#)—that is, the probability of propagation, given a certain type of SSW has been detected. This is different from the percentage of

TABLE 3. Conditional probability of propagation for the two proposed definitions. The thresholds for the AMI values are -0.6 for the time mean (lags 10–40) and -0.1 for the Δ AMI definitions. The numbers give the probability of an SSW to propagate, given it is any type (all), any type but forced with wave-1 (wave 2) topography [$m = 1$ (2)], a major sudden warming (major), a weak vortex event (weak), a displacement event (M1), or a splitting event (M2). No definition has a clear advantage over the others in predicting propagation.

Definition	Probability of propagating (%)					
	All	$m = 1$ (2)	Major	Weak	M1	M2
Time mean	25	25 (25)	25	29	26	25
Δ AMI	49	47 (51)	53	55	50	49

propagating SSWs that can be attributed to a certain event type, and it ultimately is the more important measure in terms of predictive skill. The table repeats in the first column (all) the total percentage of events across all definitions for either the absolute (time mean) or relative thresholds (Δ AMI). Then, the table gives the percentage of SSWs that are considered propagating, given that they are occurring with wave-1 ($m = 1$) or wave-2 ($m = 2$) topographic forcing, or detected as major, weak vortex, M1, or M2 events. Thus, an increased potential for detecting propagating events would translate into a conditional probability of propagation that is higher than the percentage in the “all” column.

Clearly, none of the detection criteria deviate by a large amount. In particular, splitting (M2) events are not more often propagating than the events detected by any other definition. However, we note that many of the differences between displacement versus splitting events found in literature appear in the zonally asymmetric response at the surface ([Mitchell et al. 2013](#); [Seviour et al. 2016](#)), which is not investigated in the present work.

The only definition with slightly higher propagation percentages for both thresholds is the weak vortex definition, which is probably linked to the fact that an event with a strong annular mode response at 10 hPa is more likely to also have a strong response below 20 hPa and, thus, to propagate according to our discussion above.

7. Summary and conclusions

With the help of a dry general circulation model (GCM), a large ensemble of over 1500 independent sudden stratospheric warmings (SSWs) has been investigated. The model is described in detail in [JFV14](#). With the ultimate goal of studying the typical life cycle of a generic SSW, a database of all SSWs occurring in 35 different model setups has been created by varying the

relaxation times of the Newtonian cooling, the strength of the polar vortex, and orographic forcing. These setups are purposefully chosen to span over a certain range in each parameter and to capture various model biases in comprehensive GCM studies and intraseasonal, interannual, and interhemispheric differences in observations.

In particular, the autocorrelation time scales have been computed for each setup and it was shown that they are within the range spanned by reanalysis and comprehensive climate models. Here, two observations are of particular importance: First, the main parameter impacting the autocorrelation times of the model atmosphere is the wavenumber of the surface topography, and the relaxation time scales of the Newtonian cooling scheme have only a secondary effect. Simulations with wave-1 topography generally have a shorter time scale than wave-2 topography. Second, the autocorrelation time, although important for general model variability (Gerber et al. 2008a,b), does not seem to impact the evolution of single SSWs. Indeed, there is no statistically significant difference in the evolution of SSWs coming from model setups with long versus short autocorrelation times. We think this is due to SSWs being strong and fast internally forced events, which are free to evolve under the range of time scales explored in this study.

Four definitions for SSWs have been used to detect SSWs: Major SSWs, defined as events where the temperature gradient between 60° and 90°N is inverted at 10 hPa, and which in addition include a complete reversal of the zonal-mean zonal wind at 60°N and 10 hPa (Labitzke 1981). Another definition is based on the annular mode index (AMI), and an SSW is considered to happen when the AMI at 10 hPa drops below -2.0 standard deviations (Baldwin and Dunkerton 2001; Gerber and Polvani 2009). We call these events “weak vortex events.” Finally, we detected splitting (“M2”) and displacement (“M1”) events, which are based on two-dimensional moment analysis following Mitchell et al. (2011) and using the algorithm from Seviour et al. (2013), with the thresholds of 68°N for centroid latitude and 2.4 for aspect ratio.

Creating composites for each of these definitions (with several hundreds of events each), the generic evolution for each of the definitions can be visualized. There are only small differences between the different definitions in terms of zonal-mean dynamics, similar to previous work (Yoden et al. 1999; Coughlin and Gray 2009; Palmeiro et al. 2015), who found a continuum rather than distinct types of SSWs. Furthermore, if we compare the composites of the investigated definitions (Figs. 5 and 6), the differences are very small. Comparing these definitions draws us to the conclusion that the life cycle of a typical SSW can be described in a generic

sense. However, the differences we found between downward-propagating SSWs and nonpropagating SSWs (discussed below) indicate that we might have to make a distinction, but it would have to be based on the strength of the event close to the tropopause, and not at 10 hPa where most current definitions are applied. This result is of relevance to the ongoing effort to harmonize the SSW definition (Butler et al. 2010), as it seems that for this type of investigation, where the zonal-mean large-scale dynamics is the focus, the exact definition does not matter that much. On the other hand, when looking more into detail, and in particular zonal asymmetries, other studies have found important differences among definitions, mostly between displacements and splits (e.g., Charlton and Polvani 2007; Matthewman and Esler 2011; Esler and Matthewman 2011; Mitchell et al. 2013; Seviour et al. 2016).

In the generic evolution created by compositing all distinct SSWs (Figs. 5–9), the stratosphere is in a positive annular mode phase before the onset (negative lags), in a negative phase at positive lags, and in a slightly positive phase again some 40–50 days after the event. The evolution in terms of AMI is characterized by a strong barotropic response in the stratosphere at the onset, with a tendency to persist as a weaker perturbation in the lower stratosphere and troposphere after the event. The stratospheric upward EP flux anomalies show a similarly barotropic increase throughout the stratosphere, as noted in an earlier study by Dunn-Sigouin and Shaw (2015) (Fig. 6). The tropopause height and surface pressure anomalies are synchronous and show the signature of an increased meridional overturning circulation driven by stronger EP flux divergence (Fig. 9).

The often-invoked “burst” of anomalous eddy heat flux (which is proportional to the vertical component of Eliassen–Palm flux) propagating from the surface into the stratosphere prior to the onset date (Polvani and Waugh 2004; Limpasuvan et al. 2004) is not observed with the same prominence in this study. Although the transition from positive to negative annular mode in the stratosphere is clearly accompanied (and reinforced) by anomalous upward Eliassen–Palm (EP) flux throughout the atmospheric column, the upward EP flux signal significantly exceeds its standard deviation only in the stratosphere (Fig. 6). The increased upward EP flux from the surface that is observed here is dominated by planetary waves (Fig. 7), but it is considerably smaller than the local standard deviation. Thus, even though a strong upward (planetary scale) EP flux at the surface around 1–2 weeks prior to the onset seems to be an integral part of SSW evolution, it is not a particularly strong event and could therefore not be used as a

predictor for the occurrence of an SSW. This would explain why [Dunn-Sigouin and Shaw \(2015\)](#) were able to use a threshold on upward EP flux as the only detection criterion and detected events that are similar to our SSWs, as long as it was diagnosed somewhere in the lower stratosphere.

However, the observations from the present study suggest that it is not so much an increase in tropospheric wave activity that initiates an SSW but, rather, the state of the stratospheric polar vortex that determines the propagation of existing eddies in the stratosphere. In this picture, the troposphere merely serves as reservoir for wave activity, and depending on the state of the polar vortex, more or less EP flux can propagate into the upper stratosphere. [Figure 10](#) clearly shows that the potential vorticity gradient steepens along the vortex edge long before the appearance of increased upward EP flux in both the stratosphere and the troposphere.

Concentrating on the question of “propagation” into the troposphere (i.e., strong troposphere–stratosphere coupling after the onset of an SSW), two criteria have been introduced for automatic detection, based on the AMI at 500 hPa. The first criterion uses the average AMI between 10 and 40 days after the onset, whereas the second requires a shift of mean AMI around the onset date, as determined by comparing the average AMI before and after the onset date.

At negative lags (i.e., before the event), there is only little significant difference between the propagating and the nonpropagating ensembles. Indeed, it is difficult to find any common features of propagating SSWs as the composites differ substantially for the two different criteria applied. This suggests that (at least with this kind of study) it is impossible to predict whether a potential SSW happening in the near future could be expected to propagate or not. This is in line with the findings of [Sigmund et al. \(2013\)](#), where enhanced seasonal forecast skill was only found if models are initialized at the onset, but not before.

At the onset, there is a consistent observation that propagating events have stronger negative AMI in the lower stratosphere (see [Figs. 11a](#) and [13a](#)), which differs statistically significantly from the nonpropagating composites. Similar results have been reported in earlier studies (e.g., [Hitchcock and Simpson 2014](#); [Seviour et al. 2016](#)). The same is true for the lower stratosphere at positive lags, where the propagating events show a much more persistent negative phase of the annular mode. This suggests that if at the onset date the SSW is unusually deep, and/or the lower-stratospheric perturbation persists for a longer time, the probability of sustained negative phase in the troposphere after the onset date is greater; deep events will affect the

tropopause, which in turn has direct effects on the troposphere, either by affecting the tropopause height ([Lorenz and DeWeaver 2007](#)) and/or tropospheric eddy feedbacks ([Simpson et al. 2009](#); [Kidston et al. 2015](#)).

There is no significant difference in most of the other variables. In particular, the often-invoked Eliassen–Palm flux evolution does not allow one to distinguish between the two, which casts doubt on the idea that the tropospheric EP flux plays an important part in causing SSWs to propagate or not. Similar to the discussion of differences between different SSW definitions and previous findings ([Coughlin and Gray 2009](#); [Palmeiro et al. 2015](#)), there is no indication that one particular definition preferentially selects propagating events, and the distribution of tropospheric AMI at positive lags suggests a continuum rather than a bimodal distribution with two different kinds (i.e., propagating vs non-propagating) of SSWs.

Acknowledgments. The author is grateful to Rolando Garcia for valuable comments and Edwin Gerber for both helpful comments and providing the script for autocorrelation time-scale calculations. The GCM code is freely available online ([Jucker 2015a](#)). All files necessary to run all simulations can be downloaded ([Jucker 2015c](#)), as well as the final zonal-mean SSW evolution data and analysis scripts ([Jucker 2016c](#)). Data analysis made use of the Python suite *aostools*, version 1.1 ([Jucker 2016b](#)), and *pv_atmos* ([Jucker 2014](#)), version 2.3 ([Jucker 2015b](#)). All data are also stored by the author and can be provided on request.

The author acknowledges the support of the ARC Centre of Excellence for Climate System Science (CE110001028) during the revision of this article.

This material is based on work supported by the National Science Foundation under Grants NSF-AGS-1144302 and AGS-1264195. Any opinions, findings, and conclusions or recommendations expressed in this material are those of the author and do not necessarily reflect the views of the National Science Foundation.

REFERENCES

- Albers, J. R., and T. Birner, 2014: Vortex preconditioning due to planetary and gravity waves prior to sudden stratospheric warmings. *J. Atmos. Sci.*, **71**, 4028–4054, doi:10.1175/JAS-D-14-0026.1.
- Andrews, D. G., J. R. Holton, and C. B. Leovy, 1987: *Middle Atmosphere Dynamics*. International Geophysics Series, Vol. 40, Academic Press, 489 pp.
- Baldwin, M. P., and T. J. Dunkerton, 2001: Stratospheric harbingers of anomalous weather regimes. *Science*, **294**, 581–584, doi:10.1126/science.1063315.
- , D. B. Stephenson, D. W. J. Thompson, T. J. Dunkerton, A. J. Charlton, and A. O’Neill, 2003: Stratospheric memory and

- skill of extended-range weather forecasts. *Science*, **301**, 636–640, doi:[10.1126/science.1087143](https://doi.org/10.1126/science.1087143).
- Butler, A. H., D. W. J. Thompson, and R. Heikes, 2010: The steady-state atmospheric circulation response to climate change-like thermal forcings in a simple general circulation model. *J. Climate*, **23**, 3474–3496, doi:[10.1175/2010JCLI3228.1](https://doi.org/10.1175/2010JCLI3228.1).
- , D. J. Seidel, S. C. Hardiman, N. Butchart, T. Birner, and A. Match, 2015: Defining sudden stratospheric warmings. *Bull. Amer. Meteor. Soc.*, **96**, 1913–1928, doi:[10.1175/BAMS-D-13-00173.1](https://doi.org/10.1175/BAMS-D-13-00173.1).
- Chan, C. J., and R. A. Plumb, 2009: The response to stratospheric forcing and its dependence on the state of the troposphere. *J. Atmos. Sci.*, **66**, 2107–2115, doi:[10.1175/2009JAS2937.1](https://doi.org/10.1175/2009JAS2937.1).
- Charlton, A. J., and L. M. Polvani, 2007: A new look at stratospheric sudden warmings. Part I: Climatology and modeling benchmarks. *J. Climate*, **20**, 449–469, doi:[10.1175/JCLI3996.1](https://doi.org/10.1175/JCLI3996.1).
- Charlton-Perez, A. J., and A. O'Neill, 2010: On the sensitivity of annular mode dynamics to stratospheric radiative time scales. *J. Climate*, **23**, 476–484, doi:[10.1175/2009JCLI2995.1](https://doi.org/10.1175/2009JCLI2995.1).
- Coughlin, K., and L. J. Gray, 2009: A continuum of sudden stratospheric warmings. *J. Atmos. Sci.*, **66**, 531–540, doi:[10.1175/2008JAS2792.1](https://doi.org/10.1175/2008JAS2792.1).
- Dritschel, D. G., and M. E. McIntyre, 2008: Multiple jets as PV staircases: The Phillips effect and the resilience of eddy-transport barriers. *J. Atmos. Sci.*, **65**, 855–874, doi:[10.1175/2007JAS2227.1](https://doi.org/10.1175/2007JAS2227.1).
- Dunn-Sigouin, E., and T. A. Shaw, 2015: Comparing and contrasting extreme stratospheric events, including their coupling to the tropospheric circulation. *J. Geophys. Res. Atmos.*, **120**, 1374–1390, doi:[10.1002/2014JD022116](https://doi.org/10.1002/2014JD022116).
- Edmon, Jr., H. J., B. J. Hoskins, and M. E. McIntyre, 1980: Eliassen-Palm cross sections for the troposphere. *J. Atmos. Sci.*, **37**, 2600–2616, doi:[10.1175/1520-0469\(1980\)037<2600:EPCSFT>2.0.CO;2](https://doi.org/10.1175/1520-0469(1980)037<2600:EPCSFT>2.0.CO;2).
- Esler, J. G., and N. J. Matthewman, 2011: Stratospheric sudden warmings as self-tuning resonances. Part II: Vortex displacement events. *J. Atmos. Sci.*, **68**, 2505–2523, doi:[10.1175/JAS-D-11-08.1](https://doi.org/10.1175/JAS-D-11-08.1).
- Garfinkel, C. I., D. W. Waugh, and E. P. Gerber, 2013: The effect of tropospheric jet latitude on coupling between the stratospheric polar vortex and the troposphere. *J. Climate*, **26**, 2077–2095, doi:[10.1175/JCLI-D-12-00301.1](https://doi.org/10.1175/JCLI-D-12-00301.1).
- Gerber, E. P., and L. M. Polvani, 2009: Stratosphere–troposphere coupling in a relatively simple AGCM: The importance of stratospheric variability. *J. Climate*, **22**, 1920–1933, doi:[10.1175/2008JCLI2548.1](https://doi.org/10.1175/2008JCLI2548.1).
- , —, and D. Ancukiewicz, 2008a: Annular mode time scales in the Intergovernmental Panel on Climate Change Fourth Assessment Report models. *Geophys. Res. Lett.*, **35**, L22707, doi:[10.1029/2008GL035712](https://doi.org/10.1029/2008GL035712).
- , S. Voronin, and L. M. Polvani, 2008b: Testing the annular mode autocorrelation time scale in simple atmospheric general circulation models. *Mon. Wea. Rev.*, **136**, 1523–1536, doi:[10.1175/2007MWR2211.1](https://doi.org/10.1175/2007MWR2211.1).
- , C. Orbe, and L. M. Polvani, 2009: Stratospheric influence on the tropospheric circulation revealed by idealized ensemble forecasts. *Geophys. Res. Lett.*, **36**, L24801, doi:[10.1029/2009GL040913](https://doi.org/10.1029/2009GL040913).
- Gómez-Escolar, M., N. Calvo, D. Barriopedro, and S. Fueglistaler, 2014: Tropical response to stratospheric sudden warmings and its modulation by the QBO. *J. Geophys. Res. Atmos.*, **119**, 7382–7395, doi:[10.1002/2013JD020560](https://doi.org/10.1002/2013JD020560).
- Held, I. M., and M. J. Suarez, 1994: A proposal for the intercomparison of the dynamical cores of atmospheric general circulation models. *Bull. Amer. Meteor. Soc.*, **75**, 1825–1830, doi:[10.1175/1520-0477\(1994\)075<1825:APFTIO>2.0.CO;2](https://doi.org/10.1175/1520-0477(1994)075<1825:APFTIO>2.0.CO;2).
- Hitchcock, P., and I. R. Simpson, 2014: The downward influence of stratospheric sudden warmings. *J. Atmos. Sci.*, **71**, 3856–3876, doi:[10.1175/JAS-D-14-0012.1](https://doi.org/10.1175/JAS-D-14-0012.1).
- , T. G. Shepherd, M. Taguchi, S. Yoden, and S. Noguchi, 2013: Lower-stratospheric radiative damping and polar-night jet oscillation events. *J. Atmos. Sci.*, **70**, 1391–1408, doi:[10.1175/JAS-D-12-0193.1](https://doi.org/10.1175/JAS-D-12-0193.1).
- Jucker, M., 2014: Scientific visualisation of atmospheric data with ParaView. *J. Open Res. Software*, **2**, e4–e7, doi:[10.5334/jors.al](https://doi.org/10.5334/jors.al).
- , 2015a: JFV-strat: An idealized General Circulation Model for stratosphere-troposphere coupling. Zenodo, doi:[10.5281/zenodo.18125](https://doi.org/10.5281/zenodo.18125).
- , 2015b: pv_atmos v2.3. Zenodo, doi:[10.5281/zenodo.31252](https://doi.org/10.5281/zenodo.31252).
- , 2015c: SSW runs. Figshare, doi:[10.6084/m9.figshare.1314312.v1](https://doi.org/10.6084/m9.figshare.1314312.v1).
- , 2016a: 3D Interactive Generic Sudden Stratospheric Warming composite. Zenodo, doi:[10.5281/zenodo.46174](https://doi.org/10.5281/zenodo.46174).
- , 2016b: aostools v1.1. Zendo, doi:[10.5281/zenodo.56501](https://doi.org/10.5281/zenodo.56501).
- , 2016c: Data and scripts to “Are sudden stratospheric warmings generic? Insights from an idealized GCM,” Journal of the Atmospheric Sciences (2016). Mendeley Data, doi:[10.17632/pbf8tvprfk.1](https://doi.org/10.17632/pbf8tvprfk.1).
- , S. Fueglistaler, and G. K. Vallis, 2013: Maintenance of the stratospheric structure in an idealized general circulation model. *J. Atmos. Sci.*, **70**, 3341–3358, doi:[10.1175/JAS-D-12-0305.1](https://doi.org/10.1175/JAS-D-12-0305.1).
- , —, and —, 2014: Stratospheric sudden warmings in an idealized GCM. *J. Geophys. Res. Atmos.*, **119**, 11 054–11 064, doi:[10.1002/2014JD022170](https://doi.org/10.1002/2014JD022170).
- Kidston, J., A. A. Scaife, S. C. Hardiman, D. M. Mitchell, N. Butchart, M. P. Baldwin, and L. J. Gray, 2015: Stratospheric influence on tropospheric jet streams, storm tracks and surface weather. *Nat. Geosci.*, **8**, 433–440, doi:[10.1038/ngeo2424](https://doi.org/10.1038/ngeo2424).
- Kodera, K., 2006: Influence of stratospheric sudden warming on the equatorial troposphere. *Geophys. Res. Lett.*, **33**, L06804, doi:[10.1029/2005GL024510](https://doi.org/10.1029/2005GL024510).
- Kuroda, Y., 2008: Role of the stratosphere on the predictability of medium-range weather forecast: A case study of winter 2003–2004. *Geophys. Res. Lett.*, **35**, L19701, doi:[10.1029/2008GL034902](https://doi.org/10.1029/2008GL034902).
- Kushner, P. J., and L. M. Polvani, 2004: Stratosphere–troposphere coupling in a relatively simple AGCM: The role of eddies. *J. Climate*, **17**, 629–639, doi:[10.1175/1520-0442\(2004\)017<0629:SCIARS>2.0.CO;2](https://doi.org/10.1175/1520-0442(2004)017<0629:SCIARS>2.0.CO;2).
- , and —, 2005: A very large, spontaneous stratospheric sudden warming in a simple AGCM: A prototype for the Southern Hemisphere warming of 2002? *J. Atmos. Sci.*, **62**, 890–897, doi:[10.1175/JAS-3314.1](https://doi.org/10.1175/JAS-3314.1).
- Labitzke, K., 1981: Stratospheric-mesospheric midwinter disturbances: A summary of observed characteristics. *J. Geophys. Res.*, **86**, 9665–9678, doi:[10.1029/JC086iC10p09665](https://doi.org/10.1029/JC086iC10p09665).
- Limpasuvan, V., D. W. J. Thompson, and D. L. Hartmann, 2004: The life cycle of the Northern Hemisphere sudden stratospheric warmings. *J. Climate*, **17**, 2584–2596, doi:[10.1175/1520-0442\(2004\)017<2584:TLCOTN>2.0.CO;2](https://doi.org/10.1175/1520-0442(2004)017<2584:TLCOTN>2.0.CO;2).
- Lorenz, D. J., and E. T. DeWeaver, 2007: Tropopause height and zonal wind response to global warming in the IPCC scenario integrations. *J. Geophys. Res.*, **112**, D10119, doi:[10.1029/2006JD008087](https://doi.org/10.1029/2006JD008087).
- Martius, O., L. M. Polvani, and H. C. Davies, 2009: Blocking precursors to stratospheric sudden warming events. *Geophys. Res. Lett.*, **36**, L14806, doi:[10.1029/2009GL038776](https://doi.org/10.1029/2009GL038776).
- Matsuno, T., 1971: A dynamical model of the stratospheric sudden warming. *J. Atmos. Sci.*, **28**, 1479–1494, doi:[10.1175/1520-0469\(1971\)028<1479:ADMOTS>2.0.CO;2](https://doi.org/10.1175/1520-0469(1971)028<1479:ADMOTS>2.0.CO;2).

- Matthewman, N. J., and J. G. Esler, 2011: Stratospheric sudden warmings as self-tuning resonances. Part I: Vortex splitting events. *J. Atmos. Sci.*, **68**, 2481–2504, doi:10.1175/JAS-D-11-07.1.
- McIntyre, M. E., 1982: How well do we understand the dynamics of stratospheric warmings? *J. Meteor. Soc. Japan*, **60**, 37–65.
- Mitchell, D. M., A. J. Charlton-Perez, and L. J. Gray, 2011: Characterizing the variability and extremes of the stratospheric polar vortices using 2D moment analysis. *J. Atmos. Sci.*, **68**, 1194–1213, doi:10.1175/2010JAS3555.1.
- , L. J. Gray, J. Anstey, M. P. Baldwin, and A. J. Charlton-Perez, 2013: The influence of stratospheric vortex displacements and splits on surface climate. *J. Climate*, **26**, 2668–2682, doi:10.1175/JCLI-D-12-00030.1.
- Nakagawa, K. I., and K. Yamazaki, 2006: What kind of stratospheric sudden warming propagates to the troposphere? *Geophys. Res. Lett.*, **33**, L04801, doi:10.1029/2005GL024784.
- Palmeiro, F. M., D. Barriopedro, R. García-Herrera, and N. Calvo, 2015: Comparing sudden stratospheric warming definitions in reanalysis data. *J. Climate*, **28**, 6823–6840, doi:10.1175/JCLI-D-15-0004.1.
- Polvani, L. M., and P. J. Kushner, 2002: Tropospheric response to stratospheric perturbations in a relatively simple general circulation model. *Geophys. Res. Lett.*, **29**, 40–43, doi:10.1029/2001GL014284.
- , and D. W. Waugh, 2004: Upward wave activity flux as a precursor to extreme stratospheric events and subsequent anomalous surface weather regimes. *J. Climate*, **17**, 3548–3554, doi:10.1175/1520-0442(2004)017<3548:UWFAAA>2.0.CO;2.
- Reichler, T., P. J. Kushner, and L. M. Polvani, 2005: The coupled stratosphere–troposphere response to impulsive forcing from the troposphere. *J. Atmos. Sci.*, **62**, 3337–3352, doi:10.1175/JAS3527.1.
- Ring, M. J., and R. A. Plumb, 2007: Forced annular mode patterns in a simple atmospheric general circulation model. *J. Atmos. Sci.*, **64**, 3611–3626, doi:10.1175/JAS4031.1.
- Schoeberl, M. R., 1978: Stratospheric warmings: Observations and theory. *Rev. Geophys.*, **16**, 521–538, doi:10.1029/RG016i004p00521.
- Seviour, W. J. M., D. M. Mitchell, and L. J. Gray, 2013: A practical method to identify displaced and split stratospheric polar vortex events. *Geophys. Res. Lett.*, **40**, 5268–5273, doi:10.1002/grl.50927.
- , L. J. Gray, and D. M. Mitchell, 2016: Stratospheric polar vortex splits and displacements in the high-top CMIP5 climate models. *J. Geophys. Res. Atmos.*, **121**, 1400–1413, doi:10.1002/2015JD024178.
- Sigmond, M., J. F. Scinocca, V. V. Kharin, and T. G. Shepherd, 2013: Enhanced seasonal forecast skill following stratospheric sudden warmings. *Nat. Geosci.*, **6**, 98–102, doi:10.1038/geo1698.
- Simpson, I. R., M. Blackburn, and J. D. Haigh, 2009: The role of eddies in driving the tropospheric response to stratospheric heating perturbations. *J. Atmos. Sci.*, **66**, 1347–1365, doi:10.1175/2008JAS2758.1.
- Taguchi, M., 2016: Connection of predictability of major stratospheric sudden warmings to polar vortex geometry. *Atmos. Sci. Lett.*, **17**, 33–38, doi:10.1002/asl.595.
- Tripathi, O. P., A. Charlton-Perez, M. Sigmond, and F. Vitart, 2015: Enhanced long-range forecast skill in boreal winter following stratospheric strong vortex conditions. *Environ. Res. Lett.*, **10**, 104007, doi:10.1088/1748-9326/10/10/104007.
- Woollings, T., A. Charlton-Perez, S. Ineson, A. G. Marshall, and G. Masato, 2010: Associations between stratospheric variability and tropospheric blocking. *J. Geophys. Res.*, **115**, D06108, doi:10.1029/2009JD012742.
- Yoden, S., T. Yamaga, S. Pawson, and U. Langematz, 1999: A composite analysis of the stratospheric sudden warmings simulated in a perpetual January integration of the Berlin TSM GCM. *J. Meteor. Soc. Japan*, **77**, 431–445.